JOURNAL OF MATERIALS SCIENCE 33 (1998) 4647–4655

Elastic properties of compacted metal powders

P.C. CARNAVAS
Department of Mechanical Engineering, The University of Queensland, QLD 4072, Australia
N.W. PAGE
Department of Mechanical Engineering, The University of Newcastle, NSW 2308, Australia

This paper describes a study of the unloading characteristics of compacts made from the uniaxial compression of metal powders in a cylindrical die. Spherical, irregular and dendritic copper powders and spherical stainless-steel powder were investigated to determine size, shape and material effects on the unloading response. This response was characterized in terms of Young's modulus and Poisson's ratio. Measures of these quantities were made at different relative densities by unloading from different peak axial stresses. With both parameters, there was a strong dependence on particle shape. The load response of lightly compressed material was found to be dominated by its particulate nature and interparticle forces. Unloading material in this condition gave values of Young's modulus that increased slightly and Poisson's ratio that *decreased* with increasing values of relative density. In contrast, the load response of heavily compressed material was found to be similar to that of a porous solid. Unloading material in this condition gave values of Young's modulus that increased more steeply and Poisson's ratio that *increased* with increasing values for the starting relative density. Transition between these two types of behaviour depended on the particle shape, and also, to a lesser extent, the particle material.

1. Introduction

Isostatic or rigid die pressing is commonly used in the manufacture of components from metal or ceramic powders. The load–response of the powder is important during both loading and unloading, affecting the density achieved and die or mould release behaviour. Loading of the powder mass occurs plastically involving a number of different mechanisms, which are mainly irreversible. These include relative particle movement, elastic distortion, plastic deformation and perhaps particle fracture. These mechanisms do not occur independently of one another, but are related through particle interactions that rely on the distributed and individual particle properties. In contrast, unloading of the powder mass is largely an elastic process. At the particle level, release of elastic stress would also be influenced by particle interactions dependent on geometric and physical properties of individual particles. The aim of the study reported here was to investigate the influence of particle shape, size and material effects on the elastic properties of unsintered (green) compacts of ductile metals by rigid die compaction. A companion paper [1] presents a study of the plastic behaviour during loading.

During elastic unloading, a green compact would be expected to behave as a porous body. The elastic constants for porous materials have been found in previous studies to be functions of the compact relative density, or, equivalently, the material porosity. Much of this previous work has been restricted to sintered materials at relative densities exceeding 0.70.

Measurements of the elastic modulus of porous materials made from sintered powder compacts have been made using acoustic and vibrational methods [2–7] and mechanical testing [7–10]. All results showed a strong dependence of elastic modulus on the relative density or porosity. Some [7, 10] also showed a second-order effect attributed to pore geometry.

These data have led to a number of relationships being proposed to relate the variation of elastic modulus with relative density: including linear [7, 10, 11], exponential [3, 9, 12, 13], power law [14] or polynomial [15, 16] forms. Several have considered pore geometry effects [11, 12, 16].

Less has been published concerning Poisson's ratio for these materials. Poisson's ratio for porous, sintered materials has been determined from ultrasonic measurements of elastic and shear modulus [4, 11, 15] and mechanical testing [17]. These results were for a relative density of 0.7 or higher and showed that Poisson's ratio increased monotonically with increasing relative density following a linear [15] or power law [17] dependency. Yu and co-workers [7] and [10] have performed resonant frequency and mechanical tests on sintered compacts and also used results for the elastic and shear modulus to calculate Poisson's ratio. Their results suggested that Poisson's ratio remains unchanged with variations in relative density. Brown

and Weber [9] using results from mechanical tests found that Poisson's ratio also remained constant at all porosities they explored. However, a recent model of porous materials [16], which considers the full range of relative density, predicts that at low relative density, Poisson's ratio falls with increasing relative density, but passes through a minimum before rising again.

Few studies have been reported on the elastic properties of unsintered powder compacts. Hardin and Blandford [18] have argued that loose granular material exhibits endemic plasticity. Yet Hehenberger *et al.* [19] interpreted the unloading curves of uniaxially compacted powders in terms of elastic modulus and Poission's ratio finding that, as with porous solids, the elastic modulus increased monotonically with relative density. However, in contrast to porous solids, Poisson's ratio decreased with increasing relative density. Brown and Weber [9] also found that the elastic constants were the same for unsintered (compacted) and sintered iron powders.

This paper describes a study of the unloading response of ductile metal powders of different starting morphology previously subjected to uniaxial rigid die pressing to various relative densities. This approach provided a means of identifying different mechanisms acting during unloading and their effect on the compact elastic properties. The different particle morphologies studied also provided information on the effect of different particle shapes and pore geometries on these elastic properties.

2. Experimental procedure

2.1. Description of powders studied

Details of the metal powders used for this study are shown in Table I. The spherical copper powders were supplied by *Alcan Powders and Pigments*, NJ. The irregular copper powder was supplied by *United States Bronze Powders*, NJ. The dendritic copper was supplied by *Pometon S.p.A.*, Venice, Italy. The spherical stainless steel powder was supplied by *Anval*, Torshalla, Sweden.

These powders were chosen to isolate the effects of particle size, shape and material on mechanical behaviour. The powders supplied were sieved into the seven narrowly sized powder sample identities shown in Table I to isolate particle size effects. Six of the powders consisted of particles of commercially pure copper ($> 99.5\%$ Cu), four of these were spherical powders of various size fractions, a further two were similar sizes but had particles of different morphology. The seventh powder was 316L stainless steel with near monosized, spherical particles. All of the powders were provided by their respective manufacturer in annealed condition and with no lubricants or additives.

Particle shape was quantified using computer-assisted image analysis applied to samples of the powders [20]. The shape measure shown in Table I is the "form factor" ($4\pi A/P^2$– where A is the image area and P the image perimeter).

Typical material properties for annealed commercially pure copper [21] and 316L stainless steel [22], are provided in Table II. Powders were stored under controlled atmospheric conditions at all times to ensure surface oxidation was negligible. This was confirmed using scanning electron microscopy (SEM) coupled with energy dispersive spectroscopy. SEM photographs of the powders provide further details of the particle morphologies (Fig. 1).

TABLE II Material properties

Material	Elastic modulus (GPa)	Poisson's ratio	Yield stress (MPa)	Density ($kg\,m^{-3}$)
Copper	110–120	0.35	60–80	8960
Stainless steel, (316L)	190–200	0.29	200	8000

2.2. Testing methods

Single acting uniaxial tests were performed on loose powder samples contained in a cylindrical die. The die was instrumented so that radial stress and strain, circumferential strain, and axial stress and strain could be determined. All die and punch surfaces were lubricated with graphite to ensure that the stress states recorded were close to principal stress conditions. Further details of the experimental method have been given elsewhere [1, 23].

The loading cycle continued until a pre-selected load was reached at which point unloading took place. The sample was then reloaded and subsequently unloaded at higher densities. Elastic constants were calculated from the unloading curves at the prevailing density. The maximum applied axial stress was 600 MPa.

TABLE I Details of powder systems

Powder	Method of manufacture	Particle size (μm)	Particle shape (form factor)	Vickers micro hardness, H_v
Spherical copper	Gas atomization	45 –75	0.913	55 – 67
		106 –125	0.906	75 –91
		150 –180	0.897	73 –83
		250 –300	0.897	70 –76
Irregular copper	Water atomization	150 –180	0.774	52 – 68
Dendritic copper	Electrolytic deposition	106 –125	0.609	59 –63
Spherical stainless steel (316L)	Gas atomization	106 –125	0.828	205 – 217

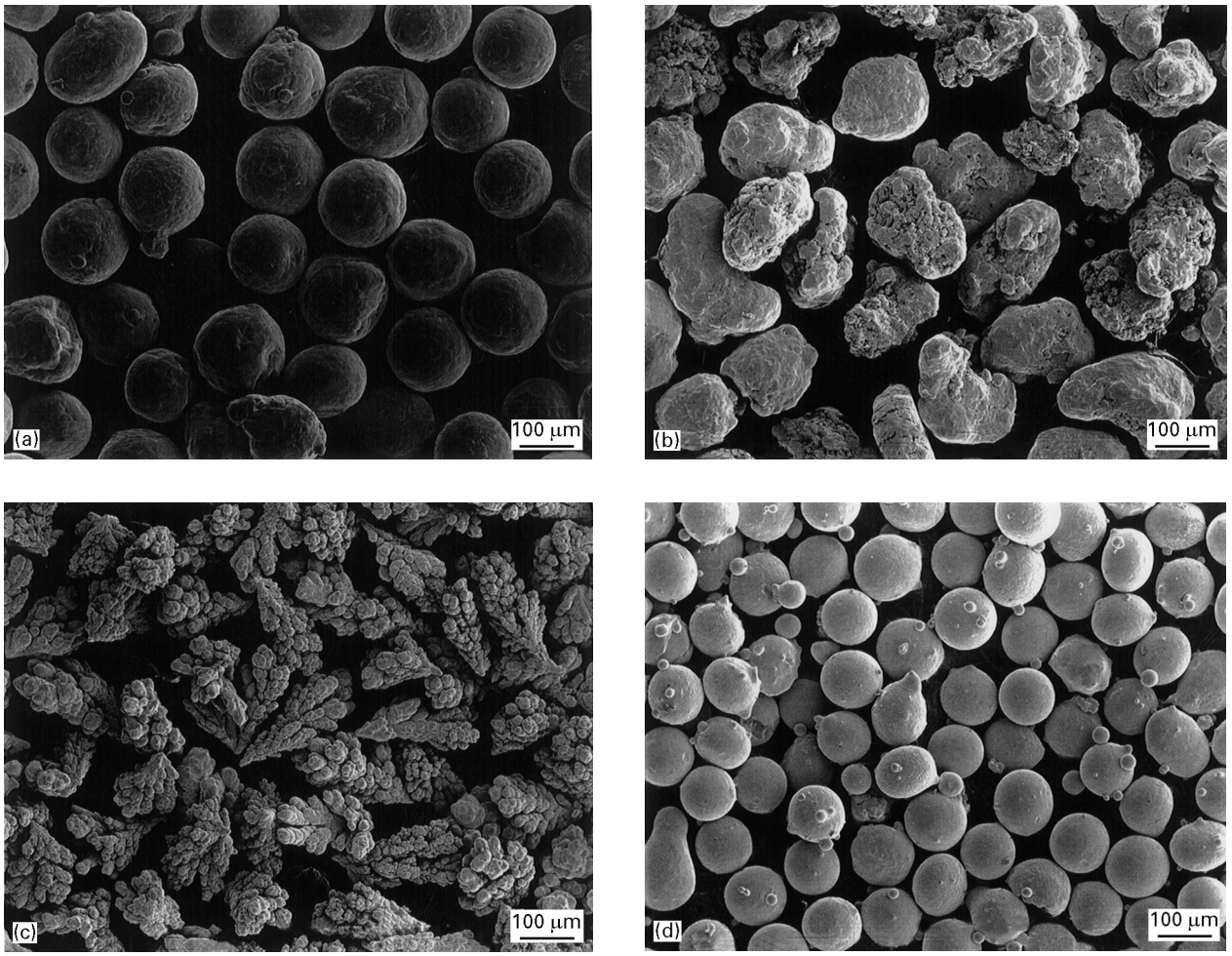

Figure 1 Typical scanning electron micrographs of the powders studied: (a) spherical copper powder (150–180 μm), (b) irregular copper powder (150–180 μm), (c) dendritic copper powder (106–125 μm), (d) spherical stainless-steel powder (106–125 μm).

3. Results

A typical unloading–reloading response is shown in Fig. 2. Plastic deformation is apparent as the non-linear behaviour at very low loads. However, both the unloading (right) curve and reloading (left) curve have parallel linear portions consistent with elastic deformation over this range. For the present purposes then, apparent elastic constants were calculated from that linear portion of the unloading response between 25 and 75% of the axial stress from which the powder was unloaded. A least squares linear regression analysis was used in this analysis.

The elastic parameters were calculated using linear elastic theory. In cylindrical co-ordinates, the triaxial stress state equations can be written as

$$\sigma_r = \frac{E}{(1+\nu)(1-2\nu)}\left[(1-\nu)\varepsilon_r + \nu(\varepsilon_z + \varepsilon_\theta)\right] \quad (1)$$

$$\sigma_z = \frac{E}{(1+\nu)\ (1-2\nu)}\left[(1-\nu)\varepsilon_z + \nu(\varepsilon_r + \varepsilon_\theta)\right] \quad (2)$$

in which E and ν are the Young's modulus and Poisson's ratio of the powder compact; σ_r and σ_z are the radial and axial stresses; and ε_θ, ε_r and ε_z are the circumferential, radial and axial stresses.

Equations 1 and 2 may be combined to give

$$\nu = \frac{\sigma_r\varepsilon_z - \sigma_z\varepsilon_r}{\sigma_r(\varepsilon_z - \varepsilon_\theta + \varepsilon_r)\ - \sigma_z(\varepsilon_r - \varepsilon_\theta - \varepsilon_z)} \quad (3)$$

As elastic properties are not time dependent and since all data were logged as time series, Poisson's ratio was conveniently determined from linearly regressed time derivatives of the quantities shown in Equation 3. Equation 2 was then solved for Young's modulus.

Axial and radial stresses and axial strain were based on direct measurement. Radial strain at the powder–die wall interface was determined assuming elastic behaviour of the die

$$\varepsilon_r = -\frac{\sigma_r}{E_d}\left(\mu\frac{\phi^2+1}{\phi^2-1} + 1\right) \quad (4)$$

where, E_d and μ are the Young's modulus and Poisson's ratio of the die material, and ϕ is the ratio of the external to internal diameter of the die.

The circumferential strain at the powder–die wall interface was found by relating the measured circumferential strain at the outer wall of the die to that at the inner wall using linear elastic thick-walled pressure vessel theory thus

$$\frac{\varepsilon_{\theta\text{inside}}}{\varepsilon_{\theta\text{outside}}} = \frac{1}{2}\left[\phi^2 + 1 + \mu(\phi^2 - 1)\right] \quad (5)$$

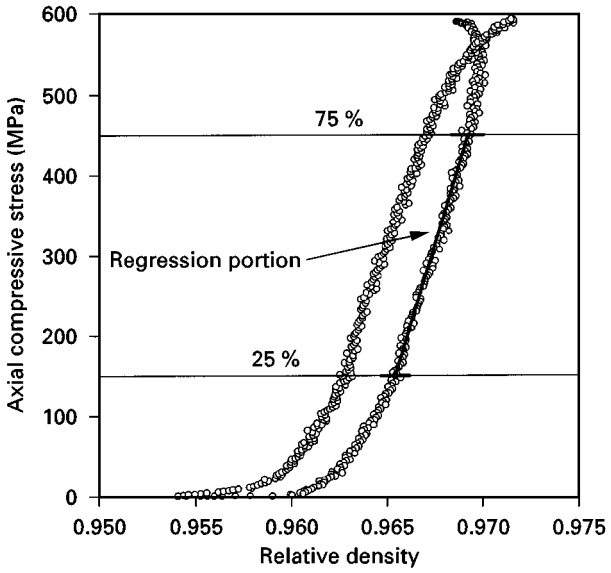

Figure 2 Typical unloading–reloading cycle showing elastic linear portions from which elastic constants were calculated.

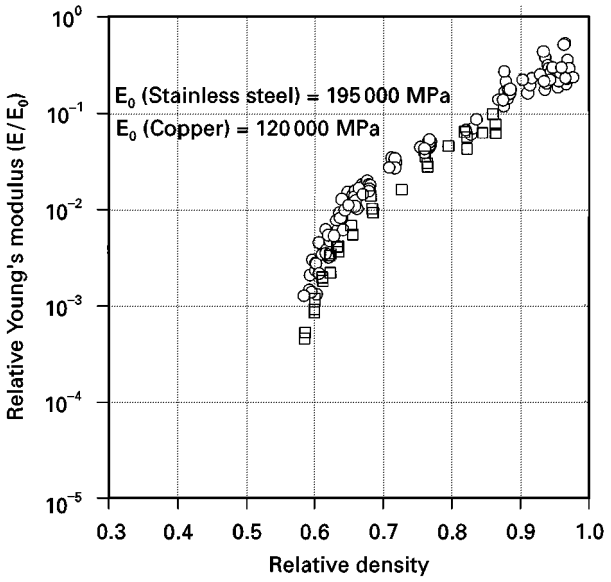

Figure 3 Relative Young's modulus for spherical copper (○) and stainless-steel (□) powders showing similar dependence on relative density (all size fractions shown).

The use of Equations 4 and 5 implicitly assumes that the radial stress exerted on the die wall by the powder is constant along the height of the compact. The validity of this assumption was based on the success of graphite release agent applied to all internal die and cap surfaces in reducing shear stresses to negligible values [1].

All spherical copper powder samples, regardless of particle size fraction, exhibited indistinguishable behaviour during the experiments. Unless otherwise noted, typical results obtained with the 150–180 μm size fraction of the spherical copper powder are presented.

4. Discussion

4.1. Modulus of elasticity

4.1.1. Effects of material

The results for all size fractions of the spherical copper and stainless-steel powders are shown in Fig. 3. The values for Young's modulus have been normalized in terms of the full density values given in Table II.

Allowing for the large scatter in the results for the spherical copper powders at high density, there was reasonable agreement between the two materials when normalized in this way. This indicates that the effect of material properties alone on the modulus of elasticity of unsintered powders can be accommodated by normalizing Young's modulus against the solid phase value.

4.1.2. Effects of particle morphology

As discussed in Section 1, a number of models have been put forward to represent the variation of Young's modulus with apparent density. To assist in the evaluation of these models, the experimental results have been plotted in a number of forms in Figs 4, 5 and 6. It can be seen from all figures that particle morphology plays an important role in the value and variation of Young's modulus with relative density.

The exponential relation of Spriggs [3] forms the basis for a class of models that have been developed. Two considered here are the original empirical relation due to Spriggs, which can be written in terms of porosity, P, as

$$\ln \frac{E}{E_0} = -aP \tag{6}$$

(where E_0 is the Young's modulus of a fully dense compact) and a higher order analytically based form due to Wang [12]

$$\ln \frac{E}{E_0} = -[aP + bP^2] \tag{7}$$

Representative curves relating these models to the experimental data are also shown in Fig. 4a–c. These curves were constrained to pass through the point $E/E_0 = 1, D = 1$ (relative density) and are therefore not necessarily the best possible fit to the data. However, they have been chosen so as to reveal the functional agreement between the models and the experimental results.

With all powders, both models could be adjusted to give reasonable agreement at high relative densities, but at the lower relative densities, neither model could follow the more rapid fall with decreasing relative density (D). This was most pronounced with the spherical powder. In terms of utility in quantitative estimation, there was little advantage in using the Wang model over the simpler Spriggs model with these materials.

The Hashin–Hasselman model is based on an analysis of a porous body with isolated pores, and can be written in the form [24]

$$\frac{E_0}{E} = 1 + c\left(\frac{1-D}{D}\right) \tag{8}$$

The experimental results have been replotted in this form in Fig. 5a–c. The Hashin–Hasselman model is

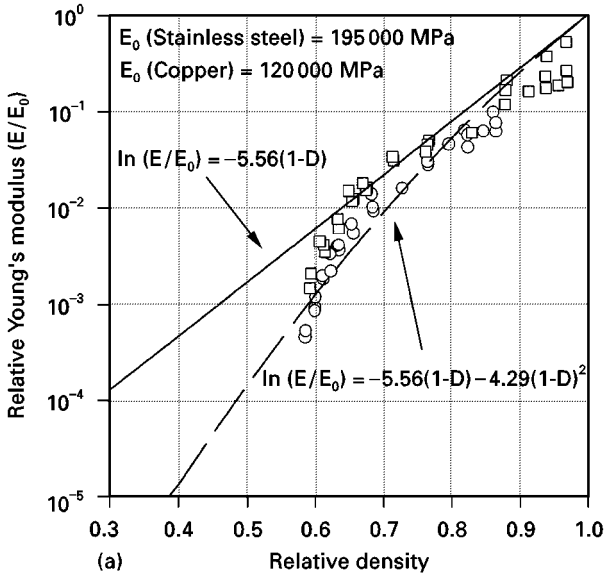

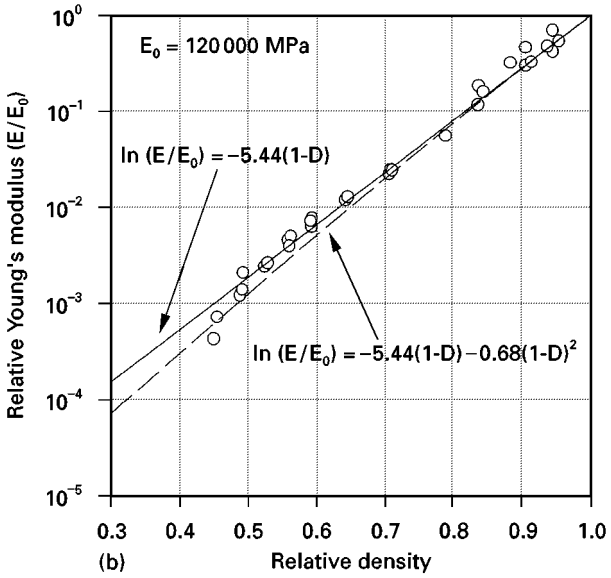

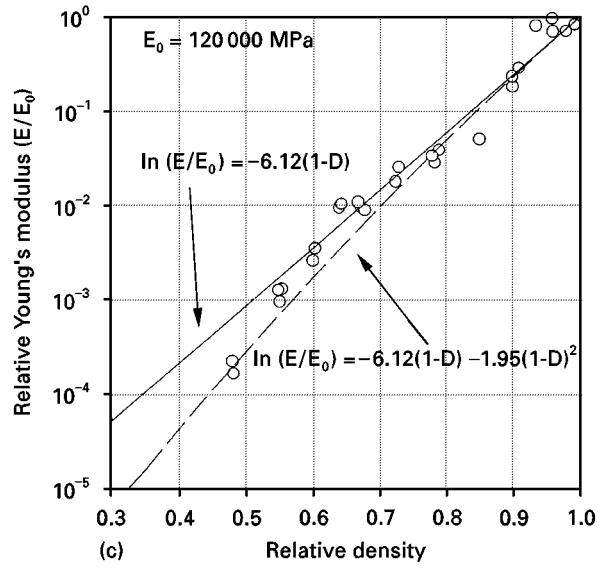

Figure 4 Relative Young's modulus on a natural log scale showing agreement with the models of Spriggs[a] and Wang[b]: parameters are shown thus (a, b): (a) spherical copper powder (5.56[a], 4.29[b]), (b) irregular copper powder (5.44[a], 0.68[b]), (c) dendritic copper powder (6.12[a],1.95[b]). ○ stainless steel; □ copper.

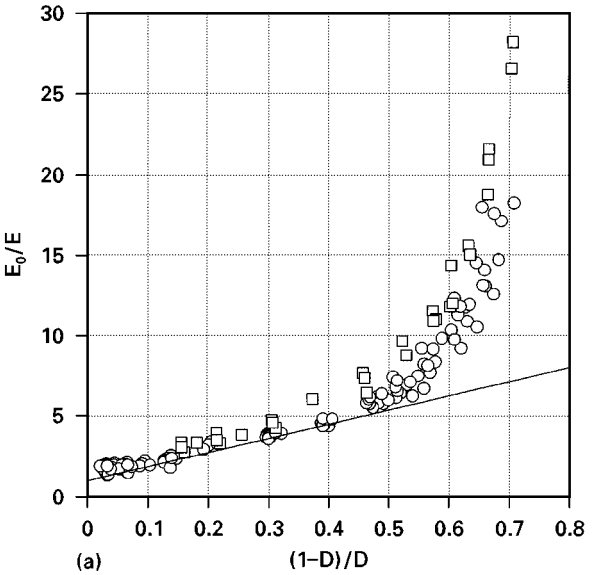

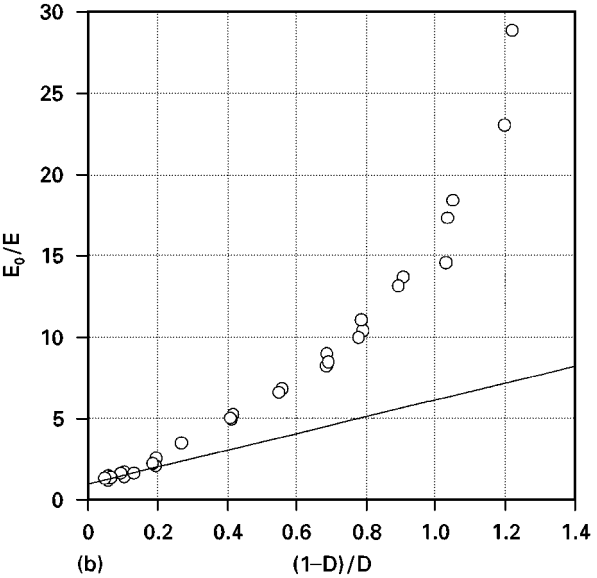

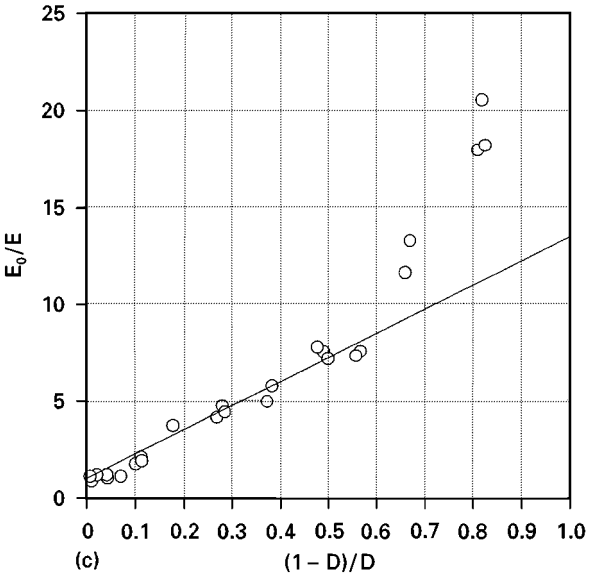

Figure 5 Inverse relative Young's modulus showing agreement with the model of Hashin–Hasselman. Line slope is model parameter c. (a) Spherical copper powder ($c = 8.75$), (b) irregular copper powder ($c = 9.00$), (c) dendritic copper powder ($c = 12.46$). ○ copper; □ stainless steel.

linear on these axes. Representative lines are shown drawn through the point $E_0/E = 1, D = 1$, the slopes of which are equal to the parameter c.

The data are most closely linear at high relative densities, the extent of linearity depending on particle morphology. Allowing for some scatter, the experimental results for the spherical powder show the most extensive linear region. It can be seen from the linear plots of data in Fig. 6a that the Hashin–Hasselman model can be used as a reasonable model for this powder morphology, for relative densities above about 0.75. At lower relative densities, the Hashin–Hasselman model overestimates Young's modulus. This model is seen to be less successful in representing the functional dependency of Young's modulus on relative density for the other two powder morphologies, underestimating Young's modulus at high densities and overestimating it at low relative densities.

From the preceding discussion, it is apparent that none of the existing models accurately describe the experimental data for all powders over the range of densities explored. Close inspection of the data in Fig. 6 shows that the data for spherical powder exhibit closely linear behaviour over the range of relative densities up to 0.95. However the data reveal a trend towards bi-linearity, as particle shape departs from sphericity. The bi-linear nature is most clearly seen in the data for the dendritic powder (Fig. 6c).

Linear segments were fitted to the results using the equation

$$\frac{E}{E_0} = k_1 D - k_2 \tag{9}$$

A least-squares algorithm was employed. Parameters for the lines of best fit are shown in Table III. Of particular note are the values of relative density at which a discontinuity in slope is evident in the cases of irregular and dendritic powders. In the parallel study of the loading behaviour of these powders [1], these points of discontinuity corresponded to recognizable transitions in the mechanism of load response. At relative densities below the discontinuity, the load response was dominated by interparticle forces and/or limited plastic deformations at points of contact, called phase 1 behaviour. The extent of the interparticle forces would have been controlled by friction and interlocking, the degree of plastic deformation was dependent on the particle material. For a given particle material, phase 1 would be most influenced by surface geometry of the powder particles. At higher relative densities, compaction behaviour was dominated by bulk plastic deformation of the particles, called phase 2 behaviour. This change in mechanism during compact loading also seems to be reflected in the elastic properties. Even without bulk movement between particles in "elastic" unloading, the relaxation of stress states in touching particle asperities by compressional unloading and bending would lead to apparently less stiff behaviour than that exhibited by the more compacted powder in which unloading would be dominated by the relaxation of stress by compressional unloading of the bulk porous material.

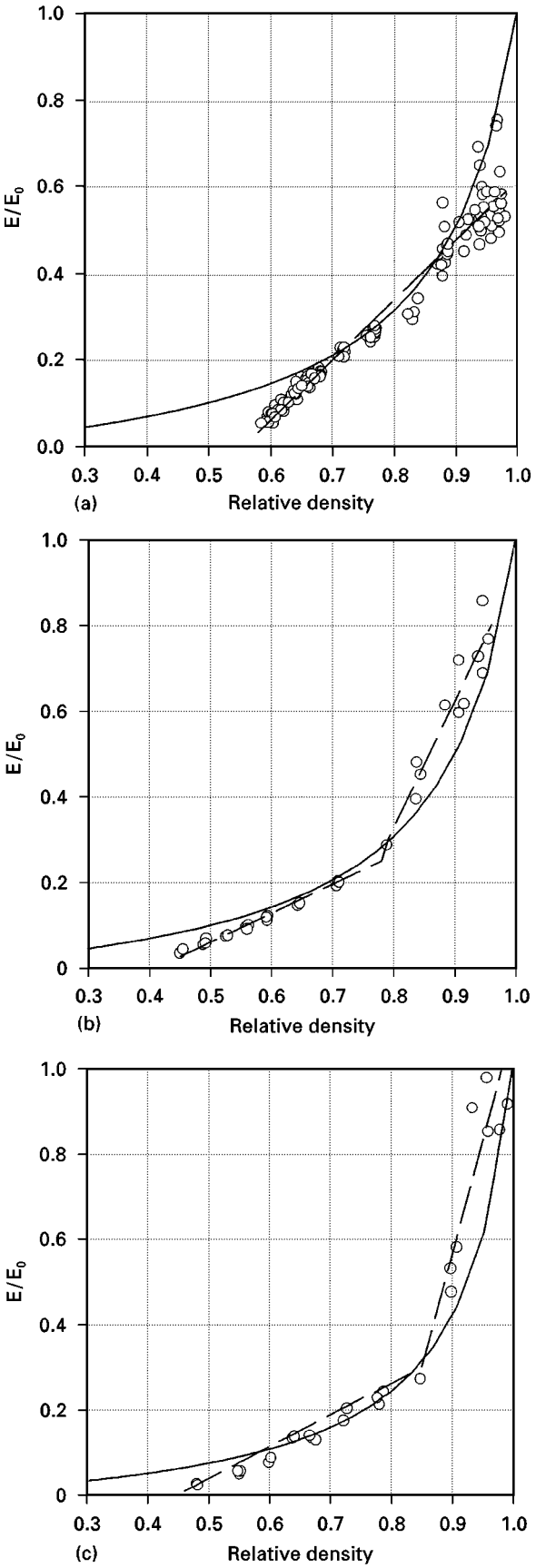

Figure 6 Young's modulus on linear axes showing agreement with Hashin–Hasselman and linear or bi-linear models: (a) spherical copper powder, (b) irregular copper powder, (c) dendritic copper powder.

4.2. Poisson's ratio

With increasing relative density, all materials showed Poisson's ratio first decreasing to a minimum value and then increasing (Figs 7 and 8). Only Hehenberger

TABLE III Results from curve fits to Young's modulus–density relationships

Powder	Density range	Details	
		k_1	k_2
Spherical copper	0.58 – 0.95	1.38	0.767
Irregular copper	0.45 – 0.78	0.675	0.275
	0.78 – 0.96	2.958	2.042
Dendritic copper	0.46 – 0.85	0.742	0.325
	0.85 – 1.00	5.267	4.175

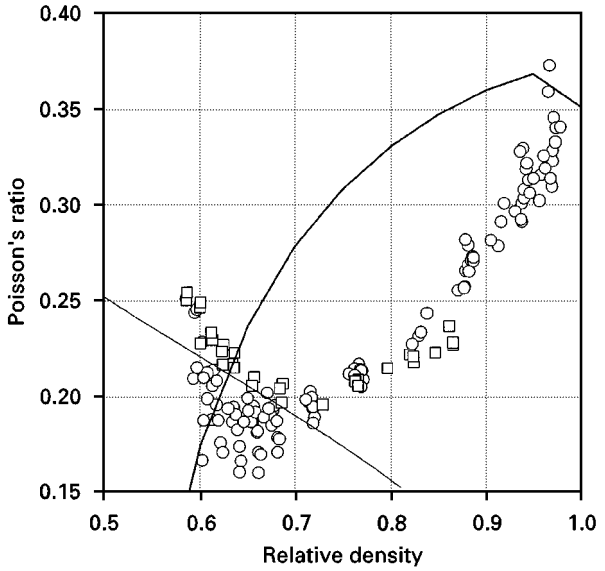

Figure 7 Poisson's ratio for spherical copper (○) and spherical stainless-steel (□) powders compared with the predictions of [16] for spherical pores in copper. Results for 106–125 μm size fractions are shown.

et al. [19] have previously reported a regime of behaviour in which Poisson's ratio fell with increasing relative density. That work was based on experiments involving cemented carbide powders. The present results, which show a fall followed by a rise with increasing relative density, provide experimental confirmation of the functional form predicted by the theory of [16]. The existence of such a transition from falling to rising behaviour with increasing relative density indicates a change in the rheological behaviour of the material. The point of transition is different for each of the powders: in the spherical copper powders, the transition occurs at a relative density of 0.65, the spherical stainless steel (Fig. 7) has its transition at a relative density about 0.70. In Fig. 8, the results comparing the copper powders of different morphologies show a transition in the behaviour of Poisson's ratio for the dendritic powder at a relative density of approximately 0.85. With the irregular copper, allowing for scatter in the data, Poisson's ratio decreases slightly for $0.45 < D < 0.6$ before ultimately rising. At the higher densities, Poisson's ratio increases with relative density for all of the powders. These transition point relative densities for the non-spherical powders correspond to those observed in the loading response

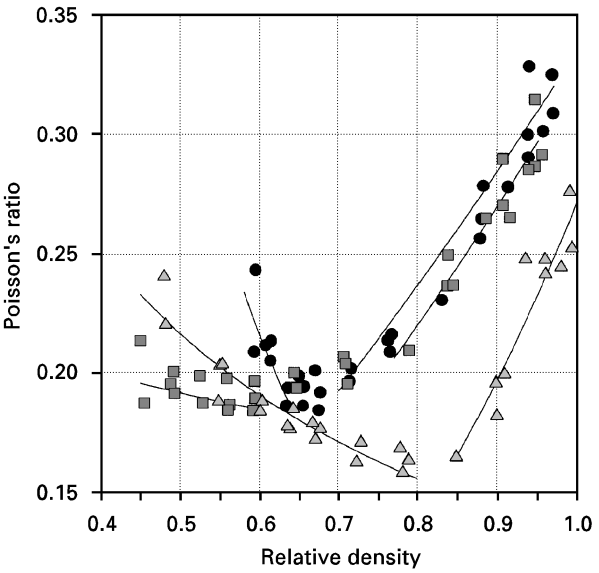

Figure 8 Poisson's ratio for copper powders of different morphology showing agreement with the polynomial forms of Kuhn and Downey [17]: (●) spherical, (■) irregular, (△) dendritic.

and the Young's modulus results discussed earlier, which mark transition from phase 1 (interparticle force and localized plastic deformation dominated) to phase 2 (bulk plastic deformation dominated) behaviour.

The results for the spherical copper and stainless-steel powders are shown in Fig. 7. These results show that the relative density at which the minima occur is material dependent – about 0.65 for the case of the copper powder and 0.70 for the stainless-steel powder. At higher relative densities, the Poisson ratio values for copper are larger than stainless steel, which reflects, in part, the relative magnitudes of the zero porosity values for these two materials ($\nu_0 = 0.35$ copper, 0.29 stainless steel). However, at lower relative density, the reverse behaviour occurs. This material dependency of the transition point between phase 1 and phase 2 behaviour is consistent with the descriptions for these phases given previously and is related to the different degrees of plastic deformation associated with each of the materials during loading [1]. The transition to phase 2 behaviour would be expected when stress levels in the bulk material approached the yield strength of the particle parent materials. This was the case here – corresponding to $D = 0.65$ for the copper and $D = 0.70$ for the stainless steel.

The theoretical variation of Poisson's ratio for porous materials with relative density has been shown by [16] to take simple mathematical form when the pores are of spherical shape. In the case of isotropic materials

$$\nu = 0.5 - \frac{E}{6K} \tag{10}$$

in which Young's modulus, E, is given by

$$E = E_0(1 - P^{2/3})^{1.21} \tag{11}$$

where $P = (1 - D)$.

TABLE IV Results from curve fits to Poisson's ratio–density relationships

	Density range	Details	
		k	n
Spherical copper	0.58 – 0.65	0.064	– 2.367
	0.70 – 0.95	0.336	1.56
Spherical stainless steel	0.58 – 0.70	0.114	– 1.446
	0.72 – 0.88	0.260	0.88
Irregular copper	0.45 – 0.60	0.168	0.214
	0.77 – 0.95	0.325	1.74
Dendritic copper	0.48 – 0.80	0.133	0.699
	0.85 – 1.00	0.273	3.07

The bulk modulus K, takes two forms. For low porosity (high relative density):

$$K_1 = K_0 \frac{2(1 - 2\nu_0)(3 - 5P)(1 - P)}{2(3 - 5P)(1 - 2\nu_0) + 3P(1 + \nu_0)} \quad (12)$$

in which subscript zero refers to the zero porosity state. For high porosity (low apparent density):

$$K_2 = K_0 \frac{2(1 - 2\nu_0)(1 - P)}{3(1 - \nu_0)} \quad (13)$$

Arnold *et al.* [16] also provided a smoothing function between these solutions, but that will not be considered here.

The results of this model evaluated using the constants for copper are shown alongside the results for 106–125 μm size fraction of the spherical copper powder in Fig. 7. In general terms, the two branches of the function give qualitative agreement with experimental results. Close quantitative agreement would not be expected since the theory is valid for spherical pore shapes and not the cusped voids between spherical particles valid for the data in Fig. 7. However, the correct prediction of a minimum suggests that this theoretical formulation offers promising scope for future study.

The measured variation of Poisson's ratio with relative density was compared with the power law relationship suggested by Kuhn and Downey [17] for porous solids

$$\nu = k(D)^n \quad (14)$$

The results of least-squares error curve fits to the data both above and below the transition point are also shown in Fig. 8 with corresponding model parameters (k, n) shown in Table IV. Both parameters show a strong dependence on powder particle shape.

5. Conclusions

The elastic properties of unsintered compacts of ductile metal powders exhibit strong dependencies on powder material, powder particle morphology and relative density, but not on particle size, at least over the range 50–300 μm in narrow size fractions of spherical powders.

The variations of both Young's modulus and Poisson's ratio with relative density showed discontinuities in gradient marking changes in the mechanics of material behaviour. The different load response characteristics were labelled phase 1 and phase 2 behaviour; phase 1 referring to changes occurring at relative densities below these discontinuities, and phase 2 above. Phase 1 was believed to be dominated by localized interparticle forces and localized plastic deformation, whereas phase 2 was believed to be dominated by bulk deformation of the particles. Phase 1 was most sensitive to particle shape effects. This two-phase elastic behaviour closely matches two-phase plastic behaviour observed in a parallel study of these same powders undergoing plastic deformation during compaction loading.

When copper and stainless-steel powders of the same size and spherical shape were compared, variations of relative Young's modulus with relative density were very similar. However, the variations in Poisson's ratio with relative density were quite distinct due to the transition between phase 1 and phase 2 behaviour occurring at different relative densities. This was attributed to the different relative strengths of the two materials.

The functional variation of Young's modulus with relative density was compared with empirical models of linear and exponential forms, as well as the theoretically based Hashin–Hasselman model. None of the fixed parameter models gave good agreement with experiment at low apparent densities. The forms of Spriggs and Wang provided good agreement to apparent densities down to as low as 0.5, depending on particle shape. The Hashin–Hasselman model best fitted the experimental data for the spherical powder. It underestimated Young's modulus at high relative densities in the irregular and dendritic powders, providing evidence of pore shape effects on the validity of this model. Bi-linear relations gave the best agreement with experiment, the discontinuities in linear segments depended on particle shape and marked the transition from phase 1 to phase 2 behaviour.

With increasing relative densities, all materials showed first a decrease in Poisson's ratio followed by an increase, thus confirming the functional form predicted from theoretical analysis by Arnold and coworkers [16]. However, the Arnold model gave poor quantitative agreement suggesting that non-spherical pore geometry effects were significant in the experiments. For all powder morphologies, the experimental data for the variation of Poisson's ratio with relative density could be approximated by different power law relations, with different parameters for phase 1 and phase 2 behaviour.

References

1. P. C. CARNAVAS and N. W. PAGE, to be published.
2. W. B. CRANDALL, (1960) see Reference [3].
3. R. M. SPRIGGS, *J. Amer. Ceram. Soc.* **44** (1961) 628.
4. S. M. LANG, (1960) see Reference [11].
5. J. A. HAGLUND and J. A. HUNTER, *J. Amer. Ceram. Soc.* **56** (1973) 327.

6. P. PANAKKAL, H. WILLEMS and W. ARNOLD, *J. Mater. Sci.* **25** (1990) 1397.
7. C. J. YU, R. J. HENRY, T. PRUCHER, S. PARTHASARATHI and J. JO, in Proceedings of Powder Metallurgy World Congress, Vol. **6** (Metal Powder Industries Association, Princeton, NJ, 1992) p. 319.
8. COBLE and KINGERY (1956) see Reference [3].
9. S. B. BROWN and G. G. A. WEBER, in "Modern Developments in Powder Metallurgy", Vol. **18–21** (Metal Powders Industry Federation, Princeton, NJ, 1988) p. 465.
10. C. J. YU and T. PRUCHER, in "Powders, Characterization, Testing and Quality Control; Advances in Powder Metallurgy and Particulate Materials, Vol. **1** (Metal Powder Industries Association, Princeton, NJ, 1993) p. 273.
11. E. A. DEAN, *J. Amer. Ceram. Soc.* **66** (1983) 847.
12. J. C. WANG, *J. Mater. Sci.* **19** (1984a) 801.
13. T. J. WATSON and J. A. WERT, *Metall. Trans. A* **24A** (1993) 2071.
14. R. M. GERMAN, "Powder Metallurgy Science", 2nd edn (Metal Powder Industries Association, Princeton, NJ, 1994).
15. A. K. MAITRA and K. K. PHANI, *J. Mater. Sci.* **29** (1994) 4415.
16. M. ARNOLD, A. R. BOCCACCINI and G. ONDAREK, *ibid.* **31** (1996) 1643.
17. H. A. KUHN and C. L. DOWNEY, *Int. J. Powder Metall.* **7** (1971) 15.
18. B. O. HARDIN and G. E. BLANDFORD, *J. Geotech. Engng* **115** (1989) 788.
19. M. HEHENBERGER, P. SAMUELSON, O. ALM, L. NILSSON and T. OLOFSSON, in IUTAM Conference on the Deformation and Failure of Granular Materials, Delft, September 1982, p. 381.
20. P. C. CARNAVAS and N. W. PAGE, in MECH-94 International Mechanical Engineering Congress, Perth, Western Australia, 15 –19 May 1994, Preprints of Papers, Vol. **2** (The Institution of Engineers Australia, 1994) p. 24.
21. B. BEVER, "Encyclopaedia of Materials Science and Engineering" (Plenum Press, New York, 1986).
22. S. KALPAKJIAN, "Manufacturing Processes for Engineering Materials" (Wiley, Chichester, 1985).
23. P. C. CARNAVAS, PhD thesis, University of Queensland (1996).
24. J. C. WANG, *J. Mater. Sci.* **19** (1984b) 809.

Received 2 December 1996
and accepted 23 June 1998